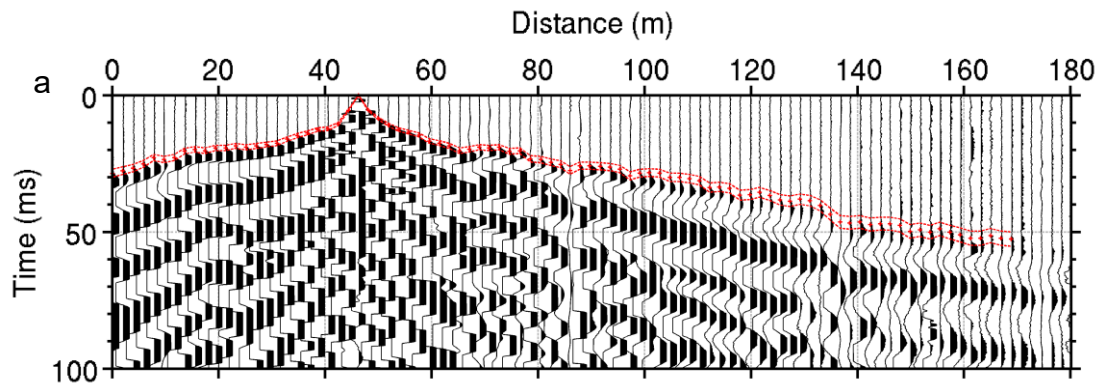


| | | | | | | | | | | |
|--------------------|-------|-------|-------|-------|-------|-------|-------|-------|-------|-------|
| Line length (m) | 286 | 286 | 286 | 190 | 190 | 142 | 142 | 190 | 190 | 190 |
| Number of shots | 30 | 30 | 30 | 25 | 25 | 19 | 19 | 25 | 25 | 25 |
| Shot spacing (m) | 10 | 10 | 10 | 8 | 8 | 8 | 8 | 8 | 8 | 8 |
| Recording time (s) | 0.75 | 0.75 | 0.75 | 0.8 | 0.8 | 0.8 | 0.8 | 0.8 | 0.8 | 0.8 |
| Sampling time (ms) | 0.125 | 0.125 | 0.125 | 0.125 | 0.125 | 0.125 | 0.125 | 0.125 | 0.125 | 0.125 |
| Time delay (s) | -0.1 | -0.1 | -0.1 | -0.05 | -0.05 | -0.05 | -0.05 | -0.05 | -0.05 | -0.05 |

First arrival times were picked manually on each shot gather. Signal-to-noise ratio varies significantly for each profile, but is mostly high enough to confidently identify first breaks up to 100-150 m distance from the source (Figure 2). This is more than enough to characterize the granite weathered zone anticipated to extend down to 10-15 m at most in such mountainous temperate catchment. The observed travel times were associated with a 5% picking error, then used to build the subsurface P-wave velocity structure (v_p) by solving an inverse problem with the pyGIMLi refraction tomography inversion module (Rücker et al., 2017). In pyGIMLi, the inversion domain corresponds to a triangular mesh with cells of constant velocity through which rays are traced using a shortest-path algorithm (Dijkstra, 1959; Moser, 1991). The velocity in each mesh cell is estimated using a generalized Gauss-Newton inversion framework. The inversion is iterative and starts with an initial model consisting of a velocity field that increases linearly with depth from [250 - 750] m/s at surface to [2000 - 5000] m/s in depth (Table S2). The velocity field is then smoothly updated at each iteration in order to reach the closest match between predicted and observed travel times. Inversions were performed with 144 combinations of starting models and regularization parameters (Table S2) in order to explore the possible solutions and estimate the uncertainty of the velocity distribution along each profile (Pasquet et al., 2016).



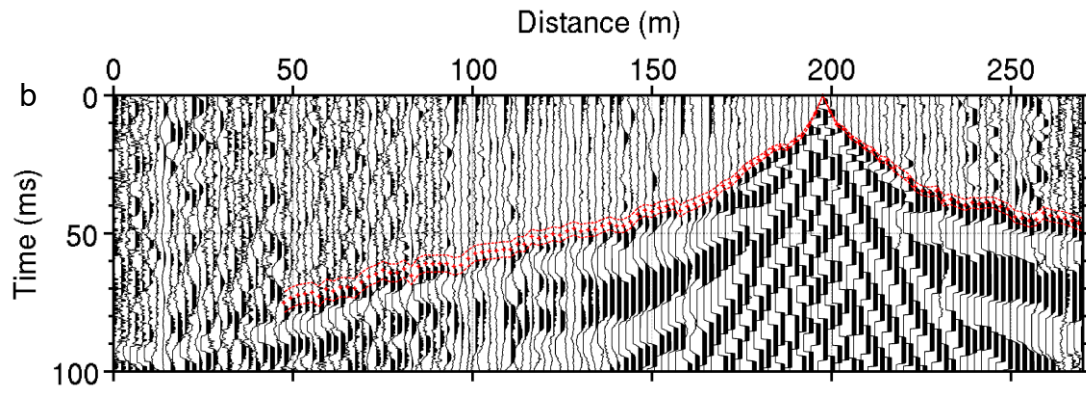


Figure 2 Examples of shots along (a) Line 15 (96 geophones) and (b) Line 1 (144 geophones).